

UC Davis

UC Davis Previously Published Works

Title

Performance of a combined optical coherence tomography and scanning laser ophthalmoscope with adaptive optics for human retinal imaging applications

Permalink

<https://escholarship.org/uc/item/1rb1d6rr>

ISBN

9781628414257

Authors

Wells-Gray, Elaine M
Zawadzki, Robert J
Finn, Susanna C
et al.

Publication Date

2015-03-13

DOI

10.1117/12.2079772

Peer reviewed

Performance of a combined optical coherence tomography and scanning laser ophthalmoscope with adaptive optics for human retinal imaging applications

Elaine M. Wells-Gray^{*a}, Robert J. Zawadzki^b, Susanna C. Finn^c, Cherry Greiner^d, John S. Werner^b, Stacey S. Choi^a and Nathan Doble^a

^a Ohio State University, College of Optometry, 338 W 10th Ave, Columbus, OH, USA 43210;

^b University of California Davis, Vision Science and Advanced Retinal Imaging Laboratory (VSRI)
UC Davis Eye Center, 4860 Y Street, Suite 2400, Sacramento, CA 95817;

^c University of Massachusetts Lowell, Lowell, MA, 01854;

^d InfraredX, 34 Third Ave, Burlington, MA, 01803

ABSTRACT

We describe the design and performance of a recently implemented retinal imaging system for the human eye that combines adaptive optics (AO) with spectral domain optical coherence tomography (OCT) and scanning laser ophthalmoscopy (SLO). The AO-OCT-SLO system simultaneously acquires SLO frames and OCT B-scans at 60 Hz with an OCT volume acquisition scan rate of 0.24 Hz. The SLO images are used to correct for eye motion during the registration of OCT B-scans. Key optical design considerations are discussed including: minimizing system aberrations through the use of off-axis relay telescopes; choice of telescope magnification based on pupil plane requirements and restrictions; and the use of dichroic beam splitters to separate and re-combine OCT and SLO beams around the non-shared horizontal scanning mirrors. We include an analysis of closed-loop AO correction on a model eye and compare these findings with system performance *in vivo*. The 2D and 3D OCT scans included in this work demonstrate the ability of this system to laterally and axially resolve individual cone photoreceptors, while the corresponding SLO images show the *en face* mosaics at the photoreceptor layer showing rods and cones. Images from both healthy and diseased retina are presented.

Keywords: Adaptive optics, Optical coherence tomography, Scanning Laser Ophthalmoscopy, Retina, Photoreceptors, Cones, Rods

1. INTRODUCTION

Adaptive optics (AO) has been used in retinal imaging as a means to enhance both lateral and axial resolution. AO was first used in a flood illuminated system by Liang et al. in 1997,¹ since then AO has been successfully applied to both scanning laser ophthalmoscopy (SLO)² and optical coherence tomography (OCT)³⁻⁶. More recently, AO systems that combine SLO and OCT into a single imaging apparatus have been implemented, including time-domain,^{7,8} spectral-domain,^{9,10} and swept-source OCT configurations.¹¹ Because SLO and OCT provide complementary views of the retina (*en face* and cross-sectional, respectively) it can be advantageous to combine both modalities into a single system. Without AO, neither modality can resolve the smallest photoreceptor structures in the eye, namely rod and foveal cone photoreceptors (both ~ 2-2.5 μm in diameter).

It is well known from diffraction theory that increasing the diameter of an imaging aperture decreases the width of the resulting point spread function (PSF), enhancing resolution. However, when imaging the eye, a large pupil comes with a significant increase in ocular aberrations that degrade the PSF. Employing AO can compensate for these aberrations, allowing imaging over a dilated pupil with the associated improvement in resolution. As an example, for a 7 mm pupil, 680 nm imaging light, and a 17 mm focal length eye, the lateral resolution limit is:

$$\Delta x = 1.22 \frac{\lambda f}{d} = 2.0 \mu m, \quad (1)$$

where λ is wavelength, f is focal length, and d is pupil diameter. The lateral resolution limit can be enhanced by an additional 38% using a confocal approach.

We have implemented a combined AO-OCT-SLO system for imaging the retina in healthy and diseased human subjects. Our goal in designing and building the system was to achieve sufficient AO correction of ocular and system aberrations to be able to resolve rods and foveal cones. In this manuscript we describe the design of our system and present images from healthy control subjects and a patient with Best disease.

2. SYSTEM DESIGN

2.1. Design Considerations

A key requirement for the AO system is that the beam at the pupil of the eye must be relayed to a number of conjugate pupil planes (PPs) throughout the system, each with individual constraints on beam diameter. At the deformable mirror (DM) pupil plane, for example, the beam should be as close to (but not greater than) 13.5 mm as possible, corresponding to the active surface area of the mirror. Similarly, at the wavefront sensor (WFS) the beam should be close to 3.4 mm. The scanning mirrors are also located in conjugate PPs, and while their sizes impose upper limits on beam size, these restraints are more flexible.

To achieve the prescribed magnifications between successive PPs required by the specific ordering of our system components, we designed a series of 4- f spherical mirror telescopes, 6 in total. These telescopes are oriented in an off-axis configuration, the specific angles of which were determined in part based on the formulation given in Gómez-Vieyra et al.¹² The off-axis design reduces system astigmatism compared to that of a planar layout. Zemax optimization routines were also used to fine-tune the incidence angles in certain telescopes (particularly the last two) such that pupil and retinal plane aberrations were minimized.

Two goals in designing the system were to achieve diffraction limited resolution over at least a 1° x 1° field of view (FOV) at the retina and to allow at least ± 3 Diopters of defocus to pass through without clipping of the beam. The AO-OCT-SLO system was modeled in Zemax to ensure design criteria such as these were met and to aid in visualizing the layout.

2.2. Current System Design

Figure 1 shows the layout of the AO-OCT-SLO imaging system. Dashed red lines indicate paths traveled by the SLO beam alone, dashed blue lines those traveled by the OCT alone, and solid red lines those where the beams are coincident. For the shared paths in Fig. 1 (solid red line) the arrow heads point in the direction the beams travel on the way to the eye. The SLO and OCT beams are combined by a custom dichroic beam splitter prior to the first spherical mirror and travel coincidentally for most of the path to and from the eye. The only exception is when they are re-split before and after their respective horizontal scanning mirrors again with dichroic beamsplitters. The 4- f relay telescopes comprise 12 silver-coated spherical mirrors with focal lengths ranging from 200 to 1000 mm. As previously mentioned, these mirrors

are arranged in an off-axis configuration with each at a different height. The schematic in Fig. 1 is an approximate birds-eye-view of the system.

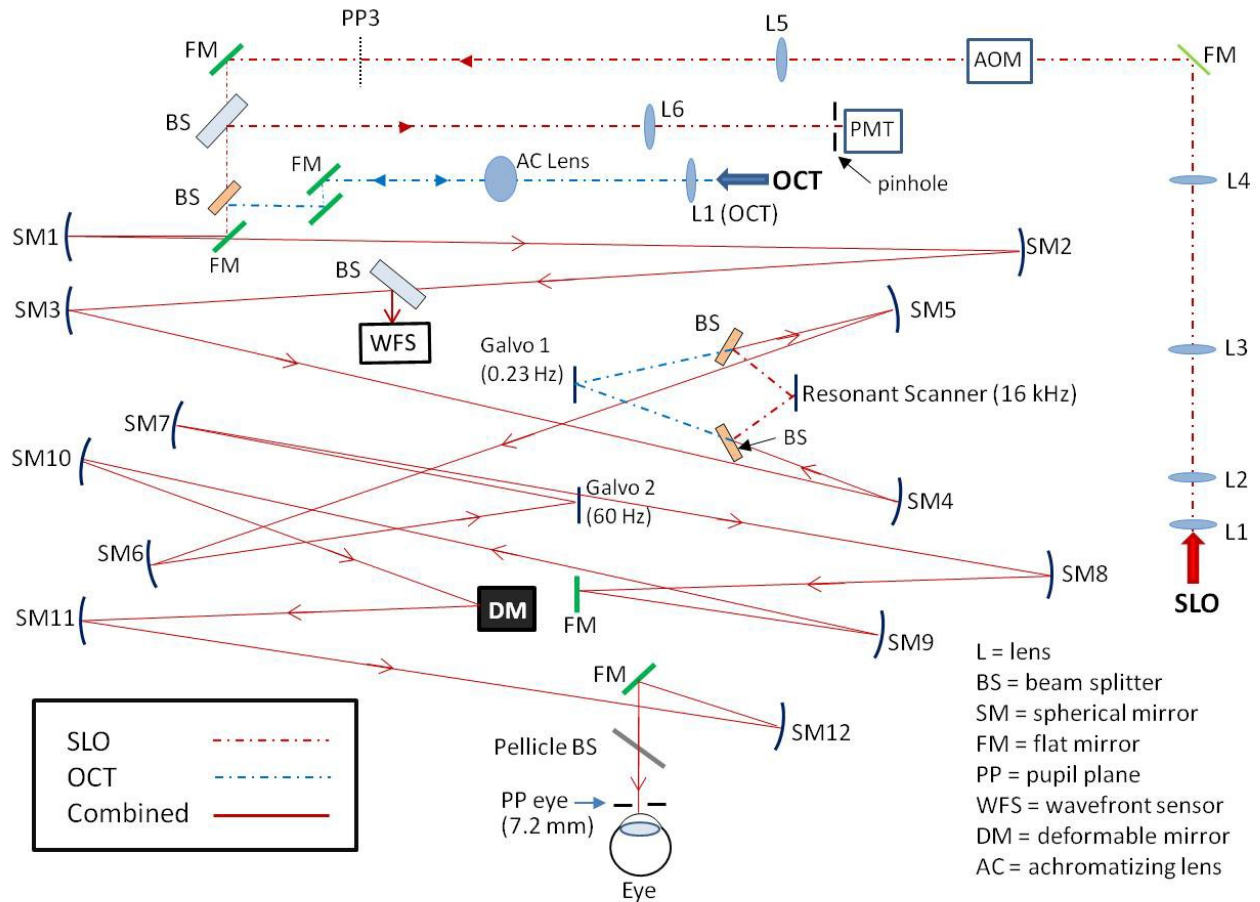


Figure 1. Diagram of the combined AO-OCT-SLO system. The OCT reference arm is not shown.

The SLO source is a 680 ± 3 nm superluminescent diode (SLD; BroadLighter T-680-HP, Superlum, Ireland). Light returning from the eye is imaged onto a PMT (H7422-50, Hamamatsu, Hamamatsu City, Shizuoka, Japan) aligned with a 1–2 Airy diameter confocal pinhole. Assuming a 17 mm focal length eye and a 7.2 mm dilated pupil (which is the largest the system is designed to accommodate), the diffraction limited resolution for the SLO sub-system calculated from Eq. 1 is $2.0 \mu\text{m}$. The OCT source is an 860 ± 70 nm SLD (BroadLighter T-860-HP, Superlum, Ireland), which is split by a 80:20 fiber coupler (AC Photonics, Santa Clara, CA), with 80% going to the reference arm and 20% to the sample arm. The reference beam (not shown in Fig. 1) is located on the main surface of the optical table, whereas the sample arm is constructed on an optical breadboard elevated 8 inches. The reference arm is constructed from elements that match the dispersion of each element in the sample arm, and a 2 cm water-filled cuvette is used to match the dispersion from the eye. Light returning from the eye is detected by the delivery fiber, recombined with that from the reference beam fiber, and then sent to the spectrometer. The spectrometer consists of a 4096 pixel CMOS camera (Sprint spL4048-140k, Basler, Ahrensburg, Germany) of which the central 2048 pixels are used. It is fitted with a grating and lens configured by

Wasatch Photonics having a 0.065 nm/pixel spacing. A custom-designed achromatizing lens in the OCT delivery path compensates for longitudinal chromatic aberration of the eye that would otherwise arise due to the wide bandwidth of the source.¹³ The OCT has a theoretical lateral resolution of 2.5 μm and axial resolution of 1.8 μm .

2.3. Scanning, Acquisition, and Processing

Three scanning mirrors are used to raster scan the beams across the retina and form the OCT and SLO images. Each beam has its own horizontal scanner, but they share a common vertical scanner. The horizontal dimension (H) of the SLO image is formed by scanning the beam laterally at 16 kHz by a resonant scanning mirror (Electro-Optical Products Corp., Ridgewood, NY). The beam is scanned vertically (V) by a 60 Hz galvo mirror (shared), yielding an SLO frame rate of 60 fps. The SLO frame dimensions are 512 (H) x 230 (V) pixels with a spatial sampling rate of 0.6 x 0.7 μm /pixel over a 1.0 x 0.5° FOV. In the SLO delivery path, the beam is modulated at 16 kHz by an acousto-optic modulator (AOM, Crystal Technology, Palo Alto, CA), which allows light to be delivered to the eye only during a portion of the forward scan of the resonant scanner.

For each SLO frame, an OCT B-scan (2-D cross-sectional slice) is simultaneously acquired at 60 Hz, though we also have the option to operate either the SLO or OCT sub-systems independently. A single B-scan comprises 601 A-scans and is formed by scanning the OCT beam spot vertically across the retina by the shared 60 Hz galvo. For a 0.5° FOV, the spatial sampling rate is 0.2 μm /pixel, though we can go up to a 2° FOV (1 μm /pixel) without under-sampling the B-scan. There is also an option to scan the OCT beam horizontally via a 0.24 Hz galvo, which allows a single OCT volume to be acquired every 4.3 s with 250 B-scans per volume.

Images are acquired using two frame grabbers housed in a single host computer: a Matrox Helios for the SLO and Matrox Solios for the OCT (Matrox, Dorval, Quebec, Canada). Synchronization of the 3 scanning mirrors and the frame grabbers is controlled through triggers generated by a custom-built timing box that uses the resonant scanner frequency as the master clock. During post-processing, SLO frames are registered and averaged using a strip-wise algorithm to remove eye motion. When the OCT spectra are converted to B-scans, a digital dispersion correction is performed which helps remove any residual dispersion mismatch that may be present in the system.¹⁴ The B-scans are then registered and averaged.

2.4 Adaptive Optics

The combined AO-OCT-SLO system uses a high-speed 97-actuator continuous-surface magnetic-membrane DM (DM97-15, ALPAO, Montbonnot, France) in combination with a Shack-Hartmann WFS (SHSCam AR-S-150-GE, Optocraft, Erlangen, Germany) to correct for system and ocular aberrations. The WFS measures the aberrations in the beam returning from the eye, and this information is used to determine the DM surface profile that is applied for correction. The DM has an active surface area of 13.5 mm and the WFS aperture is 3.4 mm. Due to the relatively large size of the DM, it was placed in the conjugate pupil plane adjacent to the eye (the next largest pupil plane) in order to avoid any greater than necessary telescope magnification (which would increase system aberrations). The WFS is placed relatively close to the detectors so that it can measure most of the system aberration. Although either the SLO or OCT beam can be used to control the AO correction when the sub-systems are operated independently, for co-acquisition, the OCT beam drives the loop, with the SLO light rejected at the WFS by a high-pass filter.

3. SYSTEM PERFORMANCE

Figure 2 shows the aberrations for the OCT and SLO beams measured with a model eye consisting of an $f=100$ mm lens and a paper target (retina) with no AO correction. The target was positioned axially so as to zero the defocus term of the SLO beam. The residual defocus in the OCT beam is due in large part to chromatic aberration introduced by the model eye lens. Also shown are the aberrations predicted by the Zemax model of the SLO system for comparison. The

measured RMS for the SLO, OCT, and also from the Zemax model were 0.12, 0.14, and 0.02 μm respectively. It should be mentioned that for this measurement, the model eye lens was slightly tilted to remove a back reflection on the WFS, which slightly increased the measured astigmatism. In addition, the DM surface is not perfectly flat when not actively controlled, further increasing the aberrations.

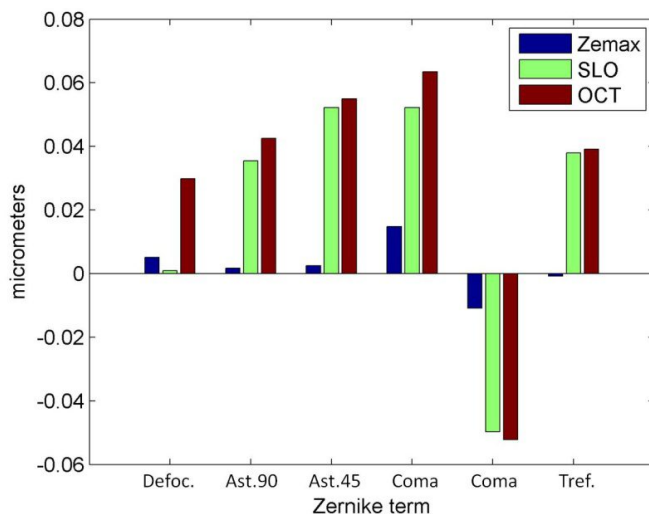


Figure 2. Zernike coefficients measured with a model eye ($f = 100$ mm). Defoc. = defocus, Ast. = astigmatism, Tref. = trefoil.

A 1951 USAF resolution test chart was used to characterize the AO-corrected resolution of the SLO sub-system. With an $f = 150$ mm lens in the model eye and a 1 Airy disk confocal pinhole, the smallest lines we could resolve were Group 6 Element 2, which have a line spacing of 14 μm . Scaled for a 17 mm focal length eye, the corresponding resolution is 1.6 μm . The improvement in resolution compared to that calculated is due to the confocal detection. While the resolution of the OCT system was not tested directly, we estimate it to be ~ 2.0 μm .

4. IMAGING RESULTS

For the results shown here, the following imaging parameters were used unless otherwise noted. The OCT power was 350 μW and the SLO power was 50 μW over a $1^\circ \times 1^\circ$ (300 x 300 μm) FOV. The confocal pinhole in front of the PMT in the SLO detection arm was 50 μm (~ 1 Airy disk). The OCT was operated in line-scanning mode (as opposed to acquiring volume scans). We focused on the photoreceptor layer by applying a defocus offset with the DM. The subject's pupil was dilated using a combination of 2.5% phenylephrine and 1% tropicamide prior to imaging. Bite bars were made using a dental impression for each subject, which along with the forehead rest reduces head motion. Subjects were asked to look at various points on the fixation target to image different retinal locations.

Figure 3 shows AO-on and AO-off OCT B-scans taken from a healthy female control subject (Subject #1) with moderate refractive error (imaged while wearing contact lenses) at 8° temporal retinal (TR) with a 1° FOV. The full B-scans (Figs. 3a and b) are displayed with a logarithmic intensity scale, while the inset on the right has linear scaling to emphasize the increased visibility of single photoreceptor structures. Each image is the average of 15 registered B-scans. The improvement in lateral resolution due to the AO correction allows clear visualization of cones both at the inner-segment/outer-segment (IS/OS) junction and at the cone outer-segment tip (COST) layers.

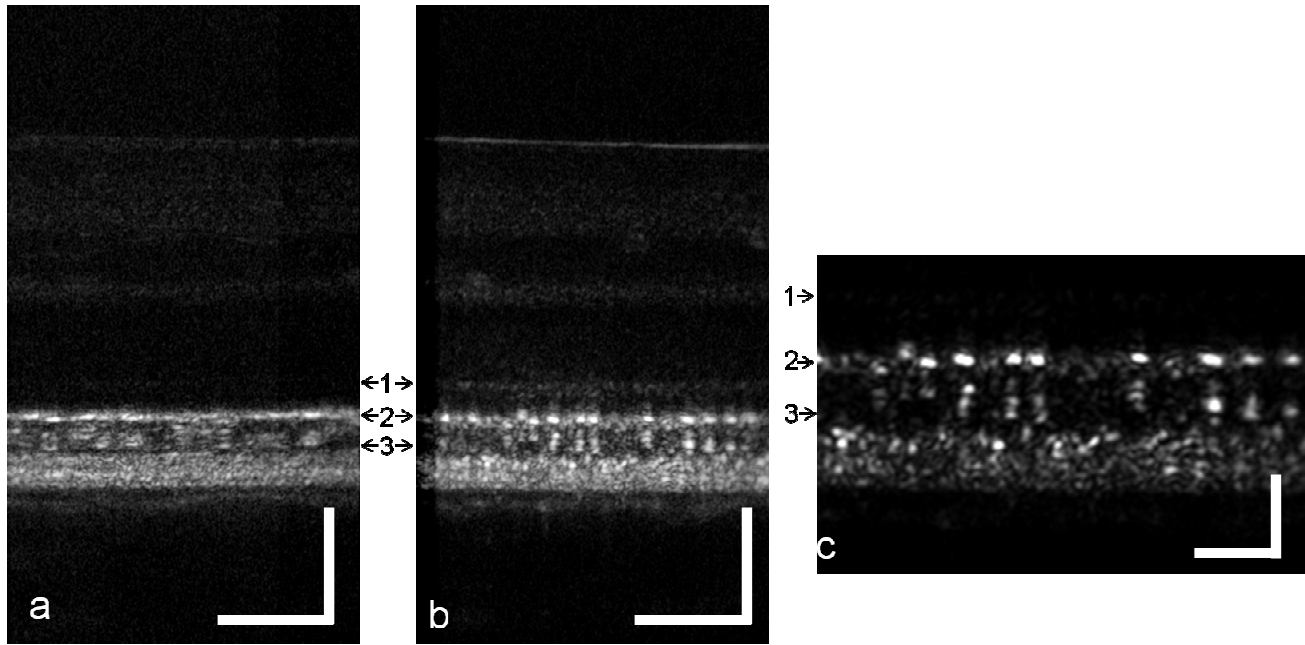


Figure 3. AO-OCT B-scans from a control subject at 8° temporal retina (TR) with plane of focus at the photoreceptor layer. (a) AO-off, log intensity scaling; (b) AO-on, log intensity scaling; (c) Photoreceptor layer AO-on displayed with linear intensity scaling. Each image is the average of 15 registered B-scans. The vertical banding toward the right of (a) and towards the left of (b) are artifacts of registering laterally shifted images. Retinal layers include: 1. external limiting membrane (ELM), 2. Inner segment / outer segment junction (IS/OS), and 3. cone outer segment tip (COST). Scale bars are 100 μm in (a) and (b), 50 μm in (c).

Figure 4 shows AO-off, AO-on, and registered SLO images from a healthy male control subject (Subject # 2, low refractive error) at 8° TR. Here the AO-on image is the average of 50 registered frames and demonstrates a striking improvement in signal-to-noise ratio. These images were taken using the SLO beam to control the AO correction (in other words with the system being operated as a stand-alone SLO imager). In the registered image, rods are resolved and seen encircling the larger, more separated cones, which is the expected structural arrangement at this eccentricity based on histology.¹⁵ The FOV for these images is 0.5° by 1°.

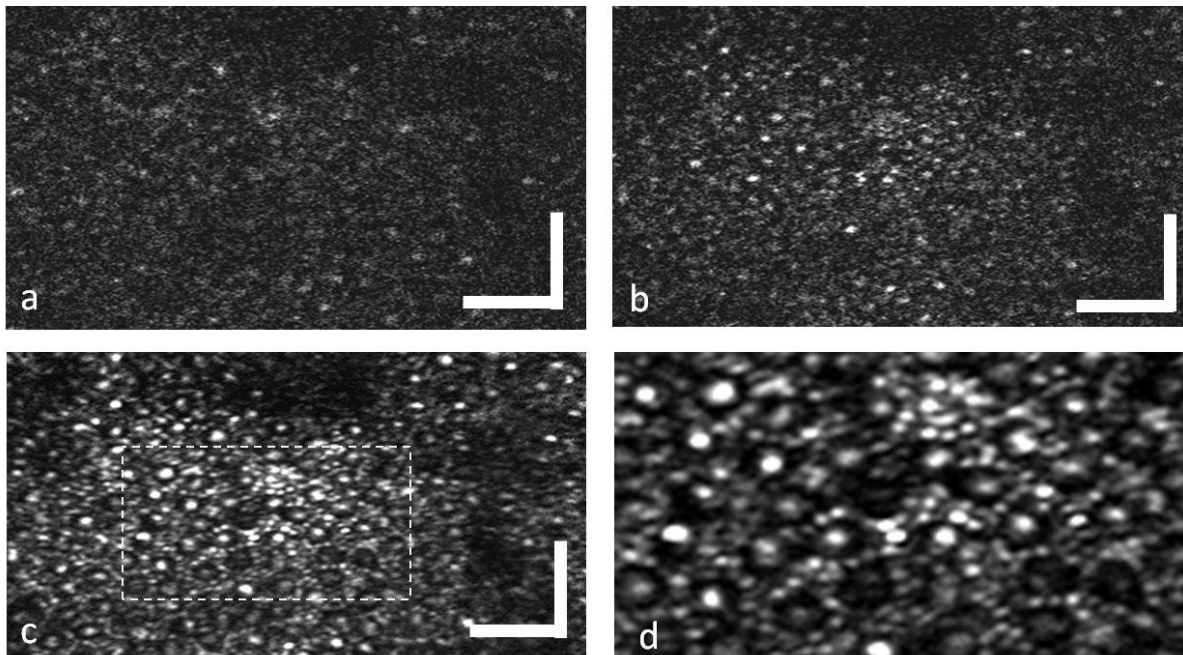


Figure 4. AO-SLO images at 8° TR from a control subject (Subject #2). (a) Single frame, AO-off; (b) Single frame, AO-on; (c) Average of 50 registered frames, AO-on; and (d) Zoomed-in view of the dashed box in (c). These were acquired using the SLO beam to drive the AO correction. Scale bar is $50\ \mu\text{m}$ and the FOV is $0.5^\circ \times 1^\circ$ except (d) which has a FOV of $0.25^\circ \times 0.5^\circ$.

In Figure 5, co-acquired OCT and SLO data are presented from a healthy male control subject (Subject #3, low refractive error) at two retinal eccentricities for which the OCT beam drove the AO loop. In the foveal images (Fig. 5a, c), cones can be resolved throughout most of the region, and in the 8° TR SLO image (Fig. 5b), rods are resolved in some areas. We observe a slight degradation in SLO resolution for the co-acquired data here when compared to the ‘stand-alone’ data shown in Fig. 4, for which the SLO beam controlled the AO correction. We attribute this to small non-common path aberrations between the OCT and SLO beam, currently on the order of $30\ \text{nm}$, which result in a less-than-optimal SLO correction when the OCT beam controls the AO. In the future, we will attempt to further reduce this mismatch with the goal of achieving the same resolution in co-acquired SLO images as we see with ‘stand-alone’ SLO.

Figure 6 shows co-acquired images from a patient with Best disease. Best disease, or Vitelliform dystrophy, is a hereditary retinal dystrophy involving the retinal pigment epithelium (RPE), and leads to a characteristic bilateral yellow ‘egg-yolk’ appearance of the macula. The subject is a 20-year-old female with low refractive error whose main symptom is a central blind spot caused by sub-retinal fluid build-up. The images in Figs. 6a and c were taken at the fovea towards the middle of the lesion; those in Figs 6b and d were taken near the periphery. The AO-OCT image from the fovea (Fig. 6a) showed that the COST layer is still present (although irregular at places) above the sub-retinal fluid, which was not clearly visible in clinical OCT images.

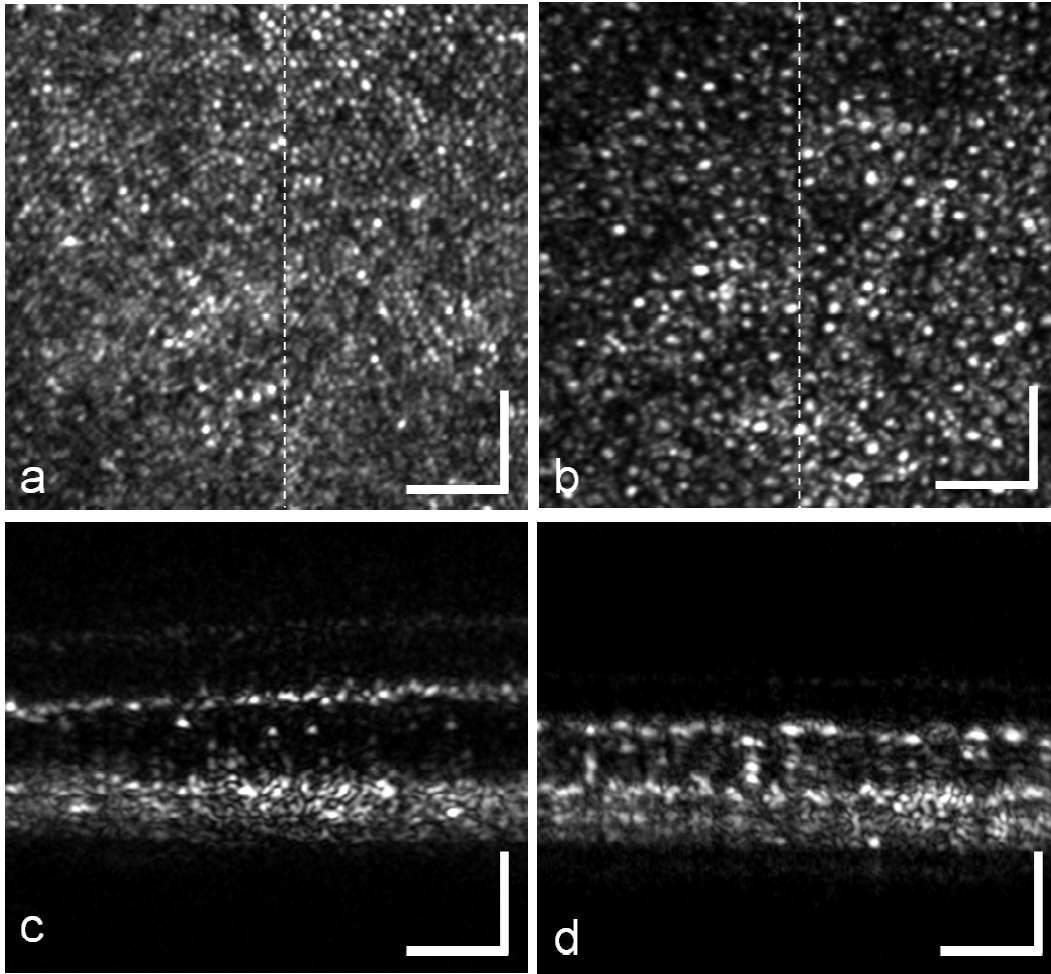


Figure 5. AO-SLO and AO-OCT images obtained in co-acquisition mode at the fovea and 8° TR for a healthy control subject (Subject #3). (a) SLO fovea, 26 frames averaged; (b) SLO 8° TR, 45 frames averaged; (c) OCT fovea, 8 frames averages; (d) OCT 8° TR, 8 frames averaged. The dashed lines in the SLO images indicate approximate orientation of the corresponding OCT slice. Scale bars are 50 μm .

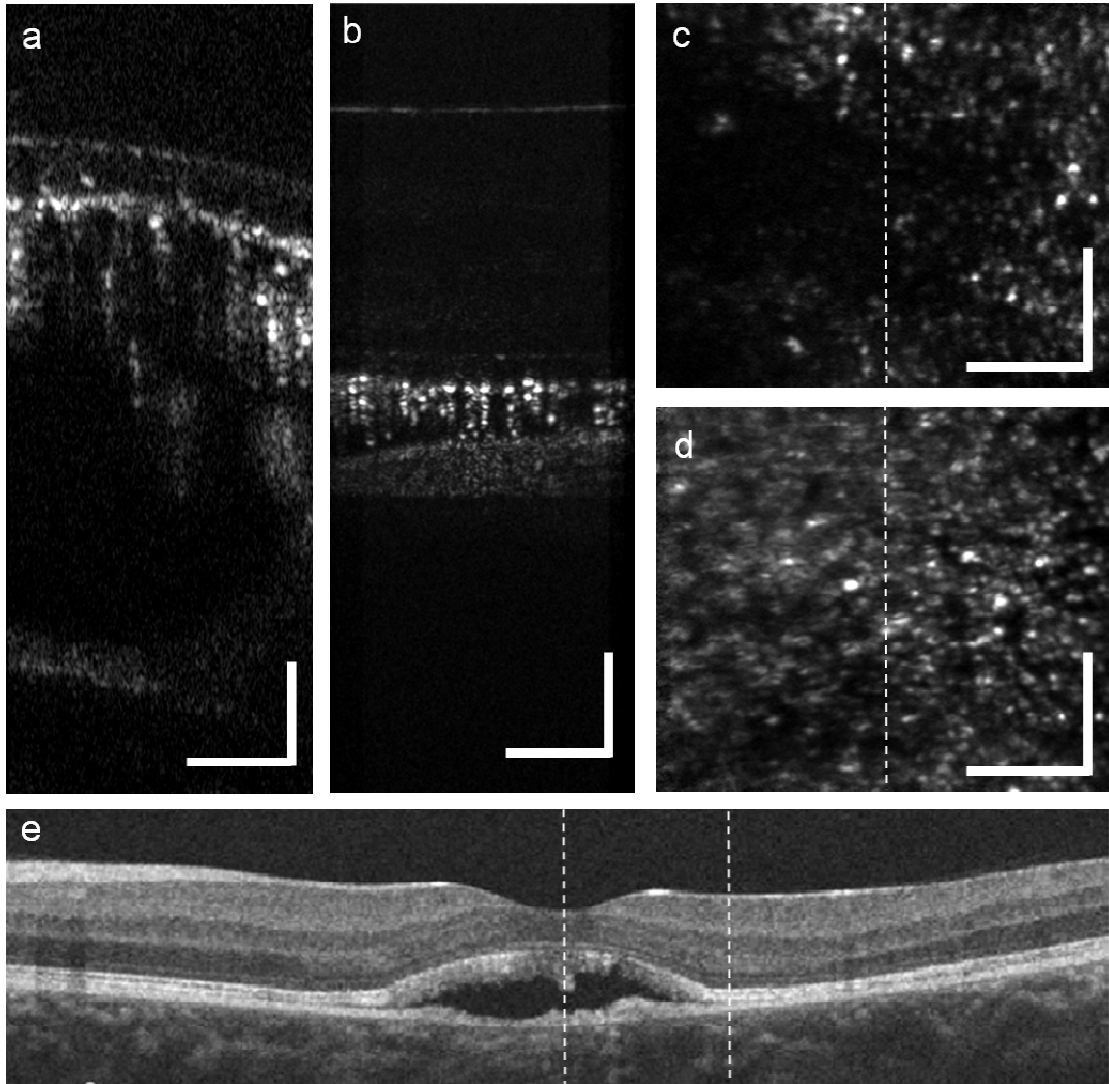


Figure 6. AO-OCT and AO-SLO images from a patient with Best Disease. (a) OCT B-scan at the fovea near the center of a fluid-filled region; (b) OCT B-scan at 3° TR near the periphery of the lesion; (c) SLO image corresponding to (a); and (d) SLO image corresponding to (b). The dashed lines in the SLO images indicate approximate orientation of the corresponding OCT slices. (e) Clinical OCT 6 mm scan with dashed lines indicating approximate locations of (a) and (b). Scale bars are 100 μm .

5. CONCLUSIONS

We have designed and implemented an AO system with combined OCT and SLO functionality for imaging the human retina. The wavefront correction provided by the AO components gives enhanced lateral resolution in both the OCT and SLO images. Results show our system is able to resolve rods in SLO images at 8° TR, and foveal cones in both the SLO and OCT images. In the future, we intend to explore the visibility of rod structure in OCT images by examining *en face* projections of OCT volume data. Further studies examining healthy retina as well as diseased populations are planned for this combined AO-OCT-SLO imaging system.

ACKNOWLEDGMENTS

This work was supported by Department of Defense (DoD) Telemedicine and Advanced Technology Research Center (TATRC) grant W81XWH-10-1-0738 (PI: Choi, SS), and NIH grants EY020901 (PI: Doble, N) and R01 EY 024239 (PI: Werner, JS).

REFERENCES

- [1] Liang, L., Williams, D.R., and Miller, D.T., "Supernormal vision and high-resolution retinal imaging through adaptive optics," *J. Opt. Soc. Am. A*, 14(11), 2884–2892 (1997).
- [2] Roorda, A., Romero-Borja, F., Donnelly, W.J., Queener, H., Hebert, T., and Campbell, M., "Adaptive optics scanning laser ophthalmoscopy," *Opt. Express*, 10(9), 405–412 (2002).
- [3] Miller, D.T., Qu, J., Jonnal, R.S., and Thorn, K.E., "Coherence gating and adaptive optics in the eye," *Proc. SPIE* 4956, 65–72 (2003).
- [4] Hermann, B., Fernández, E.J., Unterhuber, A., Sattmann, H., Fercher, A.F., Drexler, W., Prieto, P.M., and Artal, P., "Adaptive-optics ultrahigh-resolution optical coherence tomography," *Opt. Lett.*, 29(18), 2142–2144, (2004).
- [5] Zhang, Y., Rha, J., Jonnal, R., and Miller, D., "Adaptive optics parallel spectral domain optical coherence tomography for imaging the living retina," *Opt. Express*, 13(12), 4792–4811, (2005).
- [6] Zawadzki, R.J., Jones, S.M., Olivier, S.S., Zhao, M., Bower, B.A., Izatt, J.A., Choi, S., Laut, S., and Werner, J.S., "Adaptive-optics optical coherence tomography for high-resolution and high-speed 3D retinal in vivo imaging," *Opt. Express*, 13(21), 8532–8546, (2005).
- [7] Merino, D., Dainty, C., Bradu, A., and Podoleanu, A.G., "Adaptive optics enhanced simultaneous en-face optical coherence tomography and scanning laser ophthalmoscopy," *Optics Express*, 14(8), 3345–3353 (2006).
- [8] Felberer, F., Kroisamer, J., Baumann, B., Zotter, S., Schmidt-Erfurth, U., Hitzenberger, C.K., and Pircher M., "Adaptive optics SLO/OCT for 3D imaging of human photoreceptors in vivo," *Biomed. Opt. Express*, 5(2), 439–456 (2014).
- [9] Zawadzki, R.J., Jones, S.M., Pilli, S., Balderas-Mata, S., Kim, D.Y., Olivier, S.S., and Werner, J.S., "Integrated adaptive optics optical coherence tomography and adaptive optics scanning laser ophthalmoscope system for simultaneous cellular resolution in vivo retinal imaging," *Biomed. Opt. Express*, 2(6), 1674–1686, (2011).
- [10] Meadway, A., Girkin, C.A., and Zhang, Y., "A dual-modal retinal imaging system with adaptive optics," *Opt. Express*, 21(24), 29792–29807, (2013).
- [11] Mujat, M., Ferguson, R.D., Patel, A.H., Ifimia, N., Lue, N., and Hammer, D.X., "High resolution multimodal clinical ophthalmic imaging system," *Opt. Express*, 18(11), 11607–11621 (2010).
- [12] Gómez-Vieyra, A., Dubra, A., Malacara-Hernández, D., and Williams, D.R., "First-order design of off-axis reflective ophthalmic adaptive optics systems using afocal telescopes," *Opt Express*, 17(21), 18906–18919 (2009).
- [13] Zawadzki, R.J., Cense, B., Zhang, Y., Choi, S.S., Miller, D.T., and Werner, J.S., "Ultrahigh-resolution optical coherence tomography with monochromatic and chromatic aberration correction," *Opt. Express*, 16(11), 8126–8143, (2008).
- [14] Wojtkowski, M., Bajraszewski, T., Targowski, P., and Kowalczyk, A., "Real-time in vivo imaging by high-speed spectral optical coherence tomography," *Opt. Lett.*, 28(19), 1745–1747 (2003).
- [15] Curcio, C.A., Sloan, K.R., Kalina, R.E., and Hendrickson, A.E., "Human photoreceptor topography," *J. Comp. Neurol.*, 292(4), 497–523 (1990).